Available online at www.sciencedirect.com
ScienceDirect
Trans. Nonferrous Met. Soc. China 32(2022) 1896−1909
Transactions of Nonferrous Metals Society of China
www.tnmsc.cn

Corrosion resistance improvement of Ti−6Al−4V alloy by anodization in the presence of inhibitor ions

A. L. MARTINEZ[1,2], D. O. FLAMINI[1,2], S. B. SAIDMAN[1,2]

1. Instituto de Ingeniería Electroquímica y Corrosión (INIEC), Departamento de Ingeniería Química (DIQ), Universidad Nacional del Sur (UNS), Argentina;
2. Consejo Nacional de Investigaciones Científicas y Técnicas (CONICET), Bahía Blanca, Argentina

Received 22 June 2021; accepted 16 February 2022

Abstract: Colorful thin oxide films were synthesized by galvanostatic anodization on Ti−6Al−4V alloy. Three different aqueous solutions containing corrosion inorganic inhibitors (Na_2MoO_4, NaH_2PO_4 and NH_4VO_3) were employed for the anodization treatment. The effect of inhibitor anions on the corrosion behavior of the alloy in Ringer solution was studied. Open circuit potential (OCP), Tafel polarization, linear sweep voltammetry (LSV) and chronoamperometry (CA) were performed to evaluate the corrosion performance of the treated electrodes. The incorporation of the inhibitor ions was detected by the release of Mo, V and P through ICP-AES technique. The formed oxides were characterized by scanning electron microscopy (SEM), X-ray diffraction (XRD) and X-ray photoelectron spectroscopy (XPS). The results show that compact, amorphous oxides without pores or cracks were obtained independently of the solution used. The sample anodized in Na_2MoO_4 solution registered the lowest corrosion current density (0.11 μA/cm^2), and it was able to protect the alloy even after 168 h of immersion in Ringer solution. No cracks or corrosion products were detected. The XPS analysis reveals the incorporation of molybdenum to the oxide film in the form of Mo^{6+} and Mo^{4+}.
Key words: Ti−6Al−4V alloy; anodization; inorganic inhibitors; corrosion protection

1 Introduction

In the last decades, changes in lifestyle and growing life expectancy have led to an increase in the demand of orthopedic implants [1]. Thus, different polymeric, ceramic and metallic materials have been extensively investigated for enhancing their performance as medical devices.

Titanium and its alloys present some advantages over other metallic biomaterials like high specific strength, low modulus of elasticity and good corrosion resistance due to their native oxide layer that acts as a barrier between the alloy and the environment [2,3]. Ti−6Al−4V alloy was initially created for aircraft structural applications to save mass [4]. Nowadays, although the aerospace industry is the main consumer of Ti−6Al−4V alloy, other application areas like chemical, marine, industrial and biomedical industries [5−9] have incorporated the use of this alloy due to its attractive characteristics.

With respect to biomedical applications, there is concern about the release of alloying elements into the biological environment. Several reports indicate that the presence of vanadium and aluminum ions is related with health issues. For example, vanadium ions can originate an inflammatory response that causes pain and may even lead to loosening owing to osteolysis [10,11] and the presence of aluminum ions increases the probability of developing Alzheimer's disease [12]. For this reason, different techniques have been used to modify the surface of the alloy and increase its

Corresponding author: D. O. FLAMINI, E-mail: dflamini@uns.edu.ar
DOI: 10.1016/S1003-6326(22)65917-X

corrosion resistance [13−15].

Anodization or anodic oxidation is a surface modification technique employed for valve metals which allows a change on the thickness, composition and morphology of oxide layers [16,17]. It is a cheap, simple and one-step method, by which a constant voltage or current is applied between the working and counter electrodes in an electrochemical cell. Particularly for titanium and its alloys, this causes metal atoms to oxidize to Ti^{4+} ions which then combine with oxide anions from the electrolyte to progressively form an oxide layer on the metal surface [18,19]. Anodizing of titanium and its alloys can be classified into three main groups according to the characteristics of the formed oxide: traditional anodizing (thin compact films showing interference colors), anodizing in fluoride containing electrolytes (nanotubular oxides) and high voltage anodizing also called plasma electrolytic oxidation (PEO) or microarc oxidation (MAO) [20].

Previous investigation has reported that some inorganic ions such as molybdate and metavanadate can passivate titanium in sulfuric and hydrochloric acid solutions [21]. Anodizing has also been performed in phosphoric acid solutions under different conditions to improve the corrosion resistance of Ti−6Al−4V alloy in simulated physiological environment [22−24].

In this work, thin oxide films galvanostatically grew on Ti−6Al−4V alloy from three different solutions with the aim of incorporating inorganic ions into the oxide layer to improve the corrosion resistance of the substrate in Ringer solution.

2 Experimental

2.1 Materials and anodization process

The working electrode (WE) employed in this study was Ti−6Al−4V alloy in the form of rods (3 mm in diameter) axially mounted at a Teflon holder with an exposed area of 0.07 cm^2. The chemical composition of the alloy is presented in Table 1.

Table 1 Chemical composition of Ti−6Al−4V alloy (wt.%)

C	Al	V	O	N	H	Fe	Ti
0.01	6.10	4.10	0.12	0.01	0.002	0.11	Bal.

Before anodization treatment, the WE was mechanically abraded with SiC papers down to 1000 grit finish and washed with triply distilled water. Then, it was immediately introduced into a conventional three-electrode electrochemical Metrohm cell of 20 cm^3. A large Pt sheet and a saturated calomel electrode (SCE) were used as counter and reference electrodes, respectively. Unless specified otherwise, all potentials in this work are referred to SCE.

In order to evaluate the potential use of some inorganic compounds as corrosion inhibitors for the Ti−6Al−4V alloy, different electrolytes were employed: 0.50 mol/L Na_2MoO_4, 0.50 mol/L NaH_2PO_4 and 0.025 mol/L NH_4VO_3. The pH of the three solutions was adjusted to 12 by adding concentrated sodium hydroxide (NaOH) solution. All chemicals were reagent grade and solutions were made with triply distilled water. The electrodes were anodized during 1 h at a constant current of 0.05 mA employing a potentiostat-galvanostat PAR Model 273A. A rotating disk electrode EDI 101 (Radiometer Analytical S.A.) with a CTV 101 rotation rate controller (Radiometer Analytical S.A.) was used in order to avoid great oscillations in the potential versus time transients due to the oxygen evolution reaction. The rotation speed used in all cases was 500 r/min.

2.2 Corrosion performance

The corrosion performance of bare and anodized Ti−6Al−4V alloy was tested in Ringer solution (chemical composition: 0.147 mol/L NaCl, 0.00432 mol/L $CaCl_2$, and 0.00404 mol/L KCl) through different electrochemical techniques: open circuit potential (OCP), Tafel polarization, linear sweep voltammetry (LSV) and chronoamperometry (CA) measurements. The corrosion experiments were performed at 37 °C using a potentiostat-galvanostat AUTOLAB/PGSTAT128N.

Tafel tests were carried out in Ringer solution after OCP (1 h) starting from −0.20 to 0.20 V (SCE) versus OCP with a potential scan rate of 0.001 V/s. Estimation of the corrosion parameters was calculated by Tafel extrapolation method. The corrosion current density (J_{corr}) values were estimated by extrapolation of anodic and cathodic branch lines to the corrosion potential (φ_{corr}) or by extrapolation of the cathodic region of the curve to

the φ_{corr} when a non-linearity behavior was obtained in the anodic region.

All electrochemical measurements were taken at least three times for each sample and the values were turned out to be reproducible.

Ti, Al, V, P and Mo released concentrations from bare and anodized Ti−6Al−4V alloy in Ringer solution were determined using an inductively coupled plasma atomic emission spectrometer (ICP-AES) (ICPE 9000−Shimadzu Corporation, Japan).

2.3 Oxide characterization

Morphological studies of the films metallized with gold were carried out using a LEO 1450 VP scanning electron microscope (SEM) coupled with an energy dispersive X-ray spectrometer (EDX) at 20 keV of accelerating voltage.

X-ray diffraction (XRD) was used to identify the crystalline structures obtained after anodization. Diffraction patterns were obtained by a Rigaku D-Max III-C diffractometer, using Cu $K_{\alpha 1}$ (λ= 1.54059 Å) filtered with a graphite monochromator in the diffracted beam. XRD analyses were recorded in the range 2θ from 3° to 80°.

X-ray photoelectron spectroscopy (XPS) analysis was carried out in a Specs set up operating system. The XPS analysis chamber was equipped with a dual anode (Mg/Al) X-ray source and a 150 mm hemispherical electron energy analyzer (PHOIBOS) in fixed analyzer transmission (FAT) mode. Spectra were obtained with a 30 eV step energy and an Al anode operated at 100 W. The pressure during the measurement was less than 2×10^{-6} Pa. The sample was calcined in an oven at 150 °C for 30 min, then pressed, loaded onto the instrument sample holder and evacuated to ultra-high vacuum for at least 2 h before reading. It was then reduced to 350 °C for 10 min at H_2−5%Ar flow, and evacuated to ultra-high vacuum for at least 2 h before the second reading. The energies of all spectra were referenced to the C 1s peak at 285.0 eV. All the XPS spectra were deconvoluted using the CasaXPS software with a Gaussian−Lorentzian mix function.

A widefield confocal microscopy (Smartproof 5, Zeiss) was employed to estimate the thickness. ImageJ software was used to analyze the height profiles obtained from the optical images.

3 Results and discussion

3.1 Anodization process

Anodization was initially performed in a solution containing 0.50 mol/L Na_2MoO_4. After applying different currents to the Ti−6Al−4V alloy, 0.05 mA was selected since it was the lowest current that allowed a complete coating on the electrode surface easily observed to the naked eye. In order to find the best results regarding corrosion inhibition, the same current was applied to other two electrolytes: 0.50 mol/L NaH_2PO_4 and 0.025 mol/L NH_4VO_3. The treated electrodes will be identified as Ti−6Al−$4V_{0.50Mo}$, Ti−6Al−$4V_{0.50P}$ and Ti−6Al−$4V_{0.025V}$, respectively.

Figure 1 shows the potential versus time curves obtained during the anodization process. Regardless the electrolyte used, the same behavior was observed. In the first minutes, the potential increases linearly with time until it reaches the maximum, then it begins to decrease until it attains a constant value. This type of response has also been observed during the anodization of other valve metals like Nb, Al and Zr [25−27] and is representative of combined barrier/porous oxide growth.

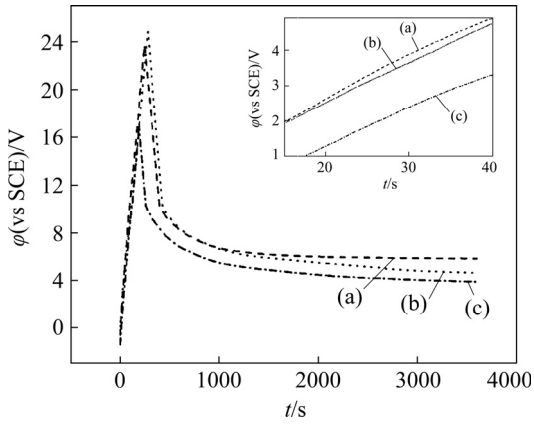

Fig. 1 Anodization of Ti−6Al−4V alloy at 0.05 mA during 1 h in different inhibitor solutions of pH 12: (a) 0.50 mol/L Na_2MoO_4; (b) 0.50 mol/L NaH_2PO_4; (c) 0.025 mol/L NH_4VO_3 (In all cases the WE was rotated at 500 r/min)

The initial increase is attributed to the growth of the barrier oxide, and the slope of the straight line indicates the rate of the coating formation: the higher the slope of potential vs time curve, the higher the rate of barrier oxide formation. The different slopes were calculated by the linear

regression through the analysis tool available in the OriginPro 8 software. The results are shown in Table 2. It can be observed that the slopes are slightly different, being the highest one corresponding to Ti−6Al−4$V_{0.50Mo}$. Therefore, different rates obtained for the oxides can be ordered in the following way: Ti−6Al−4$V_{0.50Mo}$ > Ti−6Al−4$V_{0.50P}$ > Ti−6Al−4$V_{0.025V}$. After reaching the maximum potential, the observed decrease corresponds to a loss in thickness as a consequence of the nucleation and formation of pores. In the steady state region, the anodic film thickens uniformly with time [26].

Table 2 Rates of oxide growth obtained from anodization curves

Sample	Slope/(V·s^{-1})	Standard error
Ti−6Al−4$V_{0.50Mo}$	0.108	1.41×10^{-3}
Ti−6Al−4$V_{0.50P}$	0.099	3.61×10^{-3}
Ti−6Al−4$V_{0.025V}$	0.096	$8.73\times x10^{-4}$

After the treatment, the samples were rinsed by triply distilled water and dried. The resulting electrode surface was colored to the naked eye due to the interference between light and the oxide layer. It has been proved that these resulting surface colors are dependent on the thickness of the oxide formed [18,28].

The different colored surfaces are shown in Fig. 2. A golden color was formed when the Ti−6Al−4V alloy was anodized in the solution containing molybdate ions (Fig. 2(a)); a dark golden surface was obtained when the treatment was performed in the phosphate solution (Fig. 2(b)) and a purple-blue oxide was formed when the surface of the alloy was modified in the vanadate solution (Fig. 2(c)).

(a) (b) (c)

Fig. 2 Obtained color surfaces during anodization process of Ti−6Al−4V alloy at 0.05 mA during 1 h in different inhibitor solutions of pH 12: (a) 0.50 mol/L Na_2MoO_4; (b) 0.50 mol/L NaH_2PO_4; (c) 0.025 mol/L NH_4VO_3

The colors obtained suggest that Ti−6Al−4$V_{0.50V}$ presents the thicker oxide; however, it registered the lowest final plateau voltage value. As previously mentioned, several studies have demonstrated that titanium oxide color is principally dependent on the oxide thickness. Nevertheless, SUL et al [29] have obtained oxides that presented different color surfaces with no significant differences on thickness.

3.2 Oxide characterization

In order to calculate the oxide thickness, a confocal microscope was used. For this experience, only half of the electrode surface was anodized. From the optical images (not shown), a total of 20 linear height profiles of the bare electrode/anodized interface zone were obtained and overlayed. An increase in height was observed for the anodized zone. Therefore, the oxide thickness was estimated by the difference between the average values on the treated zone and the polished region. The calculated oxide thicknesses were 5.31, 4.52 and 4.04 μm for Ti−6Al−4$V_{0.50Mo}$, Ti−6Al−4$V_{0.50P}$ and Ti−6Al−4$V_{0.025V}$, respectively. These results, combined with the colors obtained after the anodizing process, suggest that although different surface colors were observed, there were no significant differences on thickness. This is in accordance with what SUL et al [29] reported, indicating that the resultant colors can be different depending on the electrolyte used and its concentration.

The obtained oxide films were characterized by XRD (Fig. 3). In all samples, the resulting patterns show peaks that correspond to the titanium alloy. Ti−6Al−4$V_{0.025V}$ presents two rutile peaks at 62.84° and 65.44° while Ti−6Al−4$V_{0.50Mo}$ also presents a third small rutile signal at 43.84°. In the case of Ti−6Al−4$V_{0.50P}$, no peaks corresponding to crystalline titanium oxides were identified. It was proposed that phosphorus stabilizes the amorphous structure of TiO_2 [18,30]. According to the published data, TiO_2 films deposited at low temperature by most deposition methods present an amorphous phase [19,31]. Crystallization of the film is usually accomplished by heating the substrate during deposition or by a post-deposition annealing process [29,32]. Considering the XRD result, the potentials achieved during the anodizing process and the low intensity of the rutile signals, it is suggested that all the oxides are mostly formed

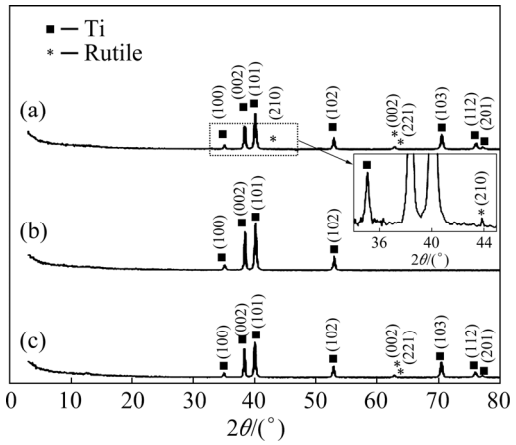

Fig. 3 XRD patterns for Ti−6Al−4$V_{0.50Mo}$ (a), Ti−6Al−4$V_{0.50P}$ (b), and Ti−6Al−4$V_{0.025V}$ (c) (Insert: magnified zone of (210) peak)

by an amorphous titanium oxide. The small signals of rutile present on Ti−6Al−4$V_{0.50Mo}$ and Ti−6Al−4$V_{0.025V}$ can be related to the fact that crystallites may nucleate in the amorphous matrix [29]. The diffraction peaks were indexed according to the JCPDS card No. 00-044-1294 and 01-073-2224 for titanium and rutile, respectively.

Moreover, a SEM analysis was performed to determine the surface characteristics of the bare and anodized Ti−6Al−4V electrodes. Figure 4 shows SEM images of the surfaces of the Ti−6Al−4V alloy before and after the anodization process. The bare alloy presents parallel lines corresponding to the mechanical grinding applied to removing the natural oxide from the alloy before the electrochemical treatment (Fig. 4(a)). After anodizing, a change in the morphology can be observed (Figs. 4(b−d)). The different anodic films cover the mechanical abrading lines and a smoothing surface is visible. The oxides extend along the entire surface and present no cracks. A more compact morphology is observed in the case of Ti−6Al−4$V_{0.50Mo}$ with respect to Ti−6Al−4$V_{0.50P}$ and Ti−6Al−4$V_{0.025V}$.

The general EDX analysis (Fig. 5) of SEM images reveals that the oxides are mostly constituted by Ti and O. It can be observed that the treated samples present the same signals of the non-anodized electrode but with a high intensity for the O signal (Figs. 5(b−d)). The alloying elements (Al and V) are also part of the oxide but their contents are difficult to be determined due to the fact that the measured signal provided by this technique could come from the bulk of the alloy [33]. Mo, P or V was not detected by EDX. This could be explained considering that their amounts are below the detection limit of the technique and due to the fact that part of the signal could come from the bulk of the alloy, as mentioned previously.

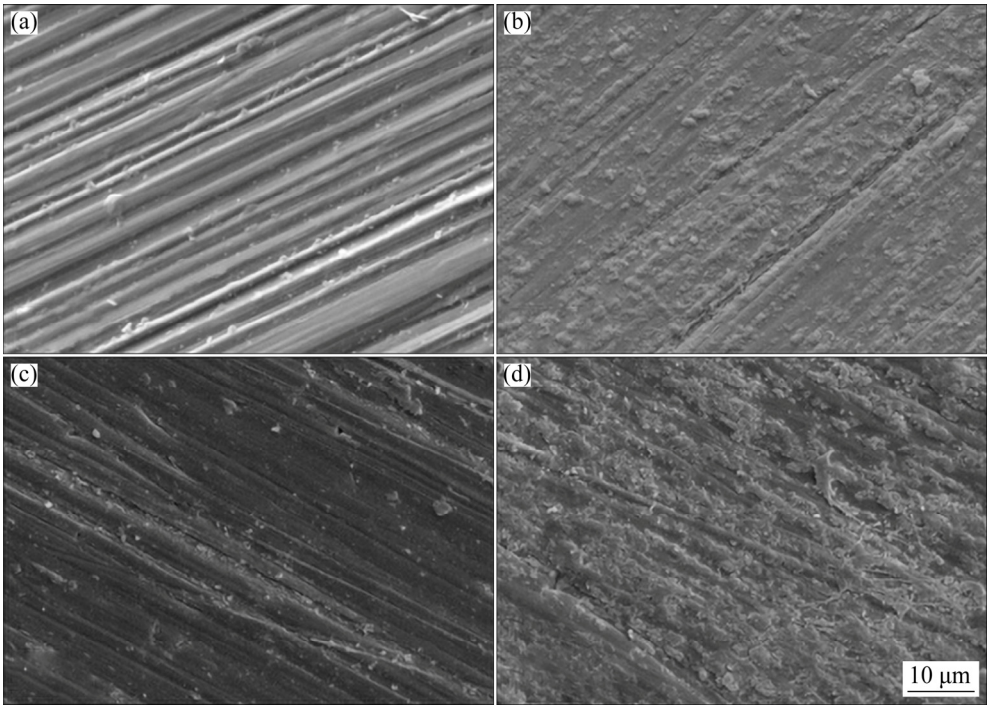

Fig. 4 SEM images of mechanically abraded Ti−6Al−4V (a), Ti−6Al−4$V_{0.50Mo}$ (b), Ti−6Al−4$V_{0.50P}$ (c), and Ti−6Al−4$V_{0.025V}$ (d)

XPS technique was employed to determine the surface chemical composition of the anodized samples. For a comparative purpose, the XPS spectrum of the bare alloy was also obtained.

The XPS spectrum of bare Ti−6Al−4V alloy reveals the presence of Ti, Al, V and O (Fig. 6(a)). On the other hand, it can be observed that the surface of Ti−6Al−4$V_{0.50Mo}$ (Fig. 6(b)) is composed

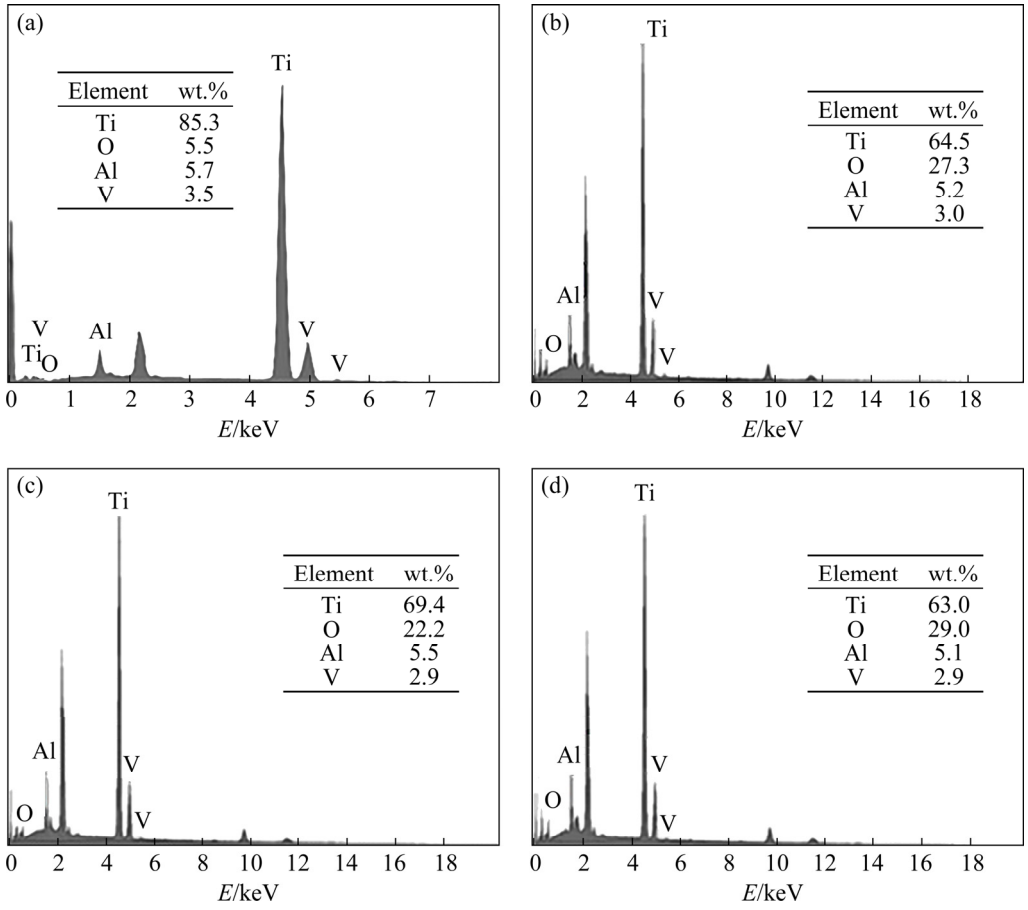

Fig. 5 EDX spectra of SEM images obtained for mechanically abraded Ti−6Al−4V (a), Ti−6Al−4$V_{0.50Mo}$ (b), Ti−6Al−4$V_{0.50P}$ (c), and Ti−6Al−4$V_{0.025V}$ (d)

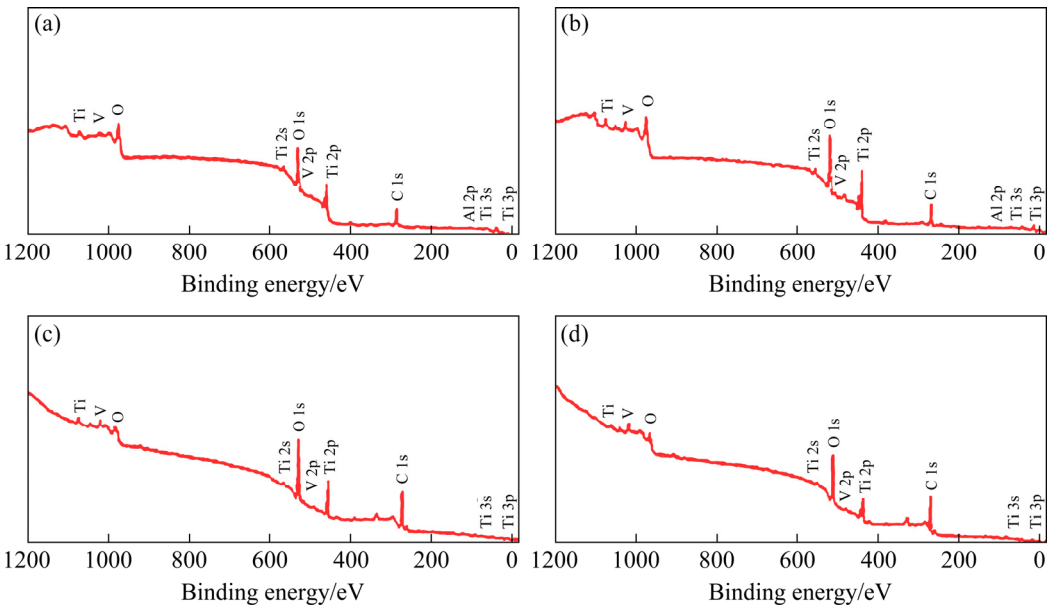

Fig. 6 XPS survey spectra of different samples: (a) Bare Ti−6Al−4V alloy; (b) Ti−6Al−4$V_{0.50Mo}$; (c) Ti−6Al−4$V_{0.50P}$; (d) Ti−6Al−4$V_{0.025V}$

of Ti, O, V, Al and Mo, while Ti−6Al−4$V_{0.50P}$ (Fig. 6(c)) and Ti−6Al−4$V_{0.025V}$ (Fig. 6(d)) only present peaks of Ti, V and O.

High resolution spectra were displayed for the elements in the anodized samples and compared with the bare alloy (Fig. 7). Figure 7(a) (Spectrum 1) shows the deconvolution of Ti 2p signals before anodization. The doublet Ti $2p_{3/2}$ (binding energy 453.9 eV) and Ti $2p_{1/2}$ (binding energy 459.6 eV) arise from spin orbit splitting. The fitting of the peaks indicates the presence of three oxidized species: Ti^{2+} (454.9 and 459.9 eV), Ti^{3+} (457.0 and 462.1 eV) and Ti^{4+} (459.4 and 465.3 eV). These results are in agreement with other publications [34,35]. After the treatment, it can be observed that for Ti−6Al−4$V_{0.50Mo}$ (Fig. 7(a), Spectrum 2), the TiO signal disappeared and the intensity of Ti_2O_3 decreased, whereas the signal of TiO_2 increased. Similar results were obtained for Ti−6Al−4$V_{0.50P}$ and Ti−6Al−4$V_{0.025V}$ (Fig. 7(a), Spectra 3 and 4) with a slightly higher signal for Ti^{3+} with respect to Ti−6Al−4$V_{0.50Mo}$.

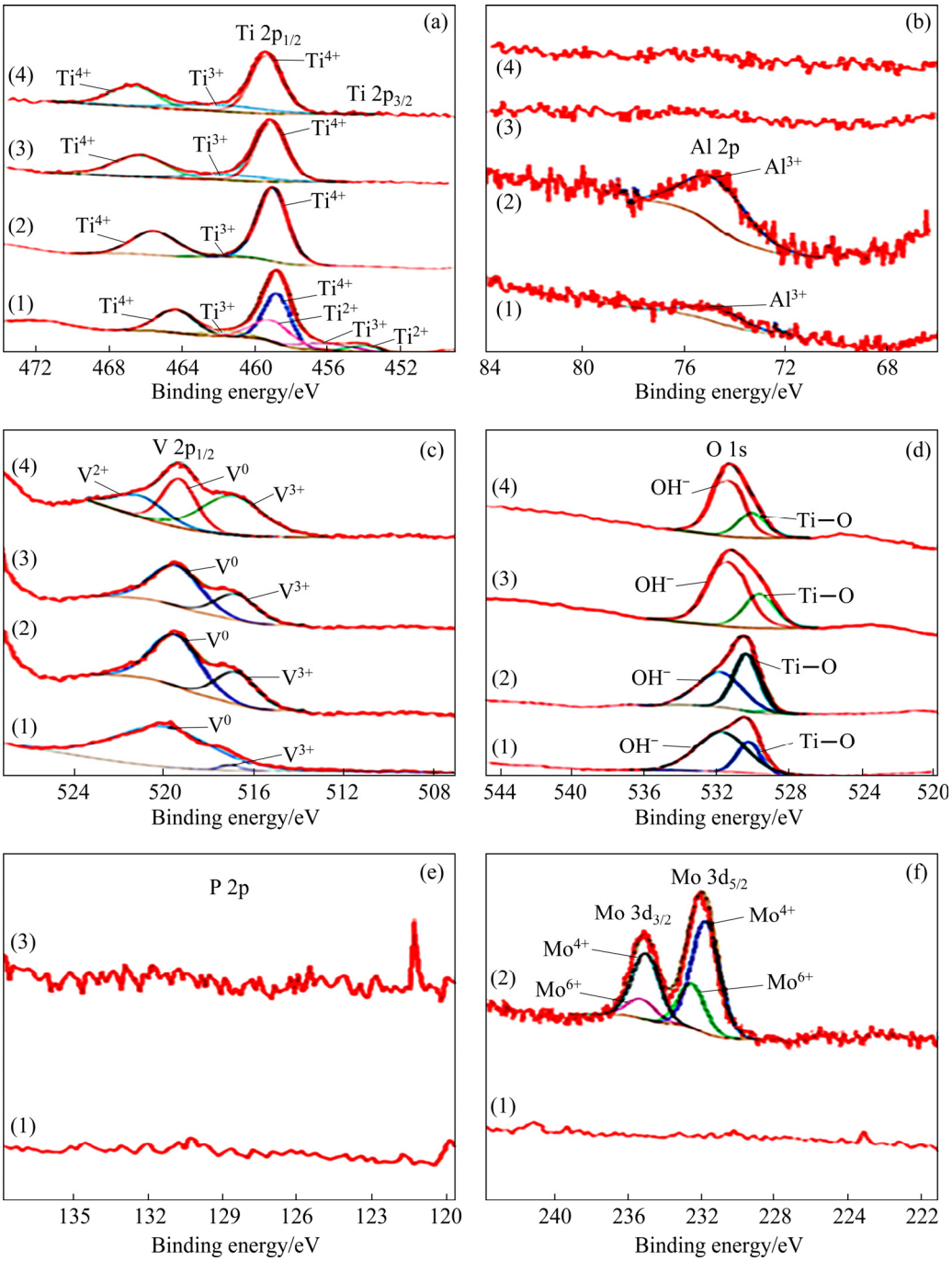

Fig. 7 High resolution of XPS spectra of Ti 2p (a), Al 2p (b), V 2p (c), O 1s (d), P 2p (e) and Mo 3d (f) for Ti−6Al−4V (1), Ti−6Al−4$V_{0.50Mo}$ (2), Ti−6Al−4$V_{0.50P}$ (3) and Ti−6Al−4$V_{0.025V}$ (4) samples

Regarding aluminum (Fig. 7(b)), a peak is presented at 74.9 eV in the bare and Ti−6Al−$4V_{0.50Mo}$ samples, it corresponds to Al^{3+} in Al_2O_3 [35]. It can be observed that the intensity of the Al 2p peak is large for Ti−6Al−$4V_{0.50Mo}$. Al 2p peak was not observed for Ti−6Al−$4V_{0.50P}$ and Ti−6Al−$4V_{0.025}$. None of the samples shows metallic Al on the surface [36].

High resolution spectrum taken in the V 2p region for the bare alloy (Fig. 7(c), Spectrum 1) shows a peak at 519.86 eV and a small signal at 516.8 eV. The first peak cannot correspond to vanadium oxides because the binding energies should be lower. According to Ref. [37], the signal could be attributed to a small amount of metallic V. Moreover, the second peak could be assigned to V_2O_3 [35,38]. After anodizing (Fig. 7(c), Spectra 2, 3 and 4), an increase in intensity is observed for V^{3+} for the treated electrodes. Particularly for Ti−6Al−$4V_{0.025V}$, a peak at 521.4 eV that could correspond to V^{2+} was also detected [39].

Figure 7(d) (Spectrum 1) shows the deconvolution of O 1s spectrum for bare Ti−6Al−4V. The analysis of the result reflects the presence of the natural oxide due to the air exposure exhibiting two sub-peaks: Ti—O link (530.6 eV) and OH^- group (531.6 eV). The presence of hydroxyl groups is due to the fact that the metallic oxide reacts spontaneously with the water molecules to form hydroxides [37,40]. After anodization the Ti oxide and OH^- groups were still detected and a small amount of Al—O (529.2 eV) was also identified for Ti−6Al−$4V_{0.50Mo}$ (Fig. 7(d), Spectrum 2) [34].

According to literature [41,42], a peak at 133.8 eV indicates the incorporation of phosphate species into the oxide layer, the spectrum for Ti−6Al−$4V_{0.50P}$ does not present any peak in the P 2p region (Fig. 7(e), Spectrum 3). ICP-AES test showed that phosphorus ions were released when the electrode was immersed in Ringer solution, but XPS technique could not detect them. This may suggest that phosphorus concentration is below the detection limit of the XPS equipment.

Finally, the Mo spectrum indicates the incorporation of Mo species in the film during anodization (Fig. 7(f)). The binding energies at 232.44 and 235.57 eV correspond to Mo^{6+} state in molybdenum trioxide (in the form of $MoO_3 \cdot H_2O$) and the peaks at 231.52 and 234.72 eV are attributed to the Mo^{4+} state in molybdenum dioxide (in the form of $MoO(OH)_2$ and MoO_2) [43]. This result confirms the incorporation of Mo into the oxide layer during the anodization process.

3.3 Corrosion performance

In order to determinate if the obtained oxides provide corrosion protection to the substrate, different electrochemical tests were performed in Ringer solution at 37 °C. OCP variation vs time was measured for the three anodized samples and compared with the bare alloy (Fig. 8). The mechanically abraded electrode registers the lowest value with an ending potential of −0.380 V (vs SCE). On the other hand, Ti−6Al−$4V_{0.50Mo}$, Ti−6Al−$4V_{0.50P}$ and Ti−6Al−$4V_{0.025V}$ present a shift toward more positive potentials ending the experience with values of 0.534, 0.407 and −0.159 V (vs SCE), respectively. These results suggest that protective oxide films were formed during anodization.

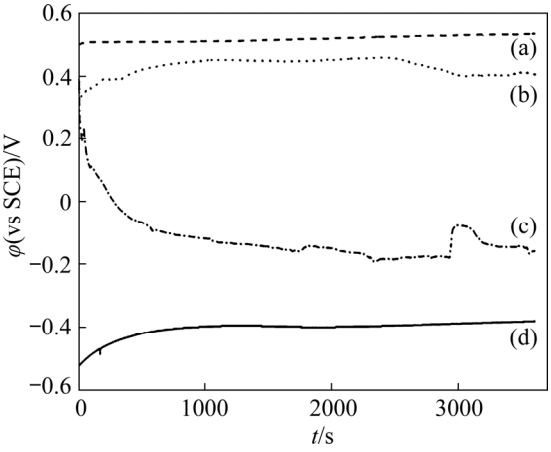

Fig. 8 Time dependence of OCP obtained in Ringer solution for different samples: (a) Ti−6Al−$4V_{0.50Mo}$; (b) Ti−6Al−$4V_{0.50P}$; (c) Ti−6Al−$4V_{0.025V}$; (d) Bare Ti−6Al−4V

The Tafel polarization curves for the bare and anodized Ti−6Al−4V electrodes in Ringer solution are plotted in Fig. 9.

The parameters obtained from Tafel polarization curves are shown in Table 3. All the treated electrodes present a shift in the φ_{corr} to more positive values compared to the untreated alloy. The greatest change is registered for Ti−6Al−$4V_{0.50Mo}$ (Fig. 9(a)) with a difference of 0.77 V with respect to the bare Ti−6Al−4V alloy (Fig. 7(d)). A decrease in the J_{corr} values can also be observed for

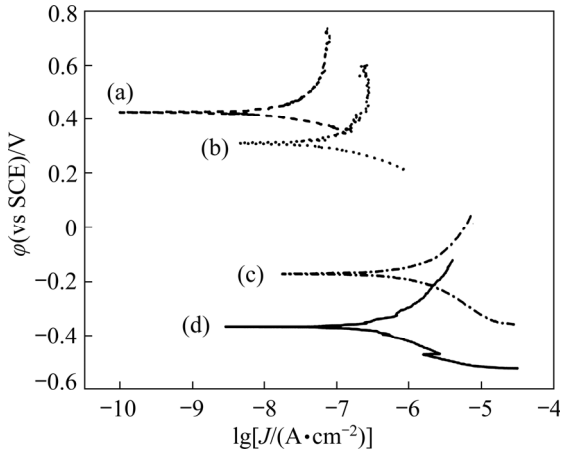

Fig. 9 Tafel polarization curves obtained in Ringer solution for different samples: (a) Ti−6Al−4V$_{0.50Mo}$; (b) Ti−6Al−4V$_{0.50P}$; (c) Ti−6Al−4V$_{0.025V}$; (d) Bare Ti−6Al−4V (Sweep rate: 0.001 V/s)

Table 3 Corrosion parameters obtained from Tafel polarization curves

Sample	φ_{corr} (vs SCE)/V	J_{corr}/ (μA·cm^{-2})	β_a/ (V·dec^{-1})	β_c/ (V·dec^{-1})
Bare Ti−6Al−4V	−0.36	5.32	1.12	0.78
Ti−6Al−4V$_{0.50Mo}$	0.41	0.11	∞	0.23
Ti−6Al−4V$_{0.50P}$	0.31	1.33	∞	0.40
Ti−6Al−4V$_{0.025V}$	−0.16	16.84	1.16	0.94

Ti−6Al−4V$_{0.50Mo}$ and Ti−6Al−4V$_{0.50P}$, being Ti−6Al−4V$_{0.50Mo}$ the one that presents the best results. On the other hand, Ti−6Al−4V$_{0.025V}$ shows the highest J_{corr}, indicating that this oxide does not contribute to the passivity of the alloy as the other coatings do. A comparison of the obtained values for the bare alloy with published data is difficult due to the fact that the corrosion current density of Ti alloys depends on surface preparation [44] among other aspects. In spite of this, the parameters for the bare alloy are in accordance with those of other research [45,46].

The values obtained for cathodic slopes indicate that oxygen reduction takes place on the metal surface. The anodic slopes for bare Ti−6Al−4V and Ti−6Al−4V$_{0.50P}$ result in similar values. However, for Ti−6Al−4V$_{0.50Mo}$ and Ti−6Al−4V$_{0.50P}$, a non-linearity behavior was obtained due to the small active dissolution zone and the passivation achieved by the alloy in the anodic region. In these particular cases, an infinite value results from the calculation of anodic slopes. The Tafel extrapolation method is still valid if one of the branches of the polarization curves is under activation control. In these cases, considering the behavior of the anodic branches, the J_{corr} values were estimated by extrapolation of the anodic Tafel lines to the φ_{corr} [47,48].

Figure 10 shows the polarization curves for the anodized and non-anodized samples. The anodic branch of the curves shows an active−passive transition for both the bare and the treated samples. The obtained passivation current densities for Ti−6Al−4V$_{0.50Mo}$, Ti−6Al−4V$_{0.50P}$, Ti−6Al−4V$_{0.025V}$ are 99, 1565 and 1125 nA/cm^2, respectively. After a passivation plateau, all current densities start to increase probably due to the oxygen and chlorine evolution reactions that take place at approximately 1.5 V (vs SCE) [49]. Even though the polarization was performed up to 3.0 V (vs SCE) no breakdown potential was detected. Moreover, there is a shift in the corrosion potential to nobler values for Ti−6Al−4V$_{0.50Mo}$ and Ti−6Al−4V$_{0.50P}$; only in the case of Ti−6Al−4V$_{0.50Mo}$, a decrease in the corrosion current density is observed.

It is important to analyze the potential range between 0.4 and 0.5 V (vs Ag/AgCl). VELTEN et al [50] defined this zone as the body potential and it corresponds to the oxidation−reduction potential of the body fluid. It can be observed that the current

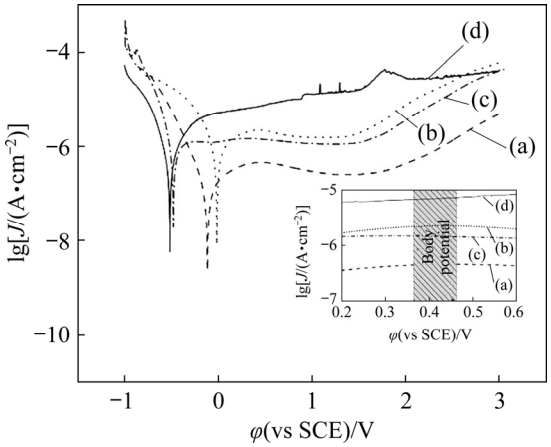

Fig. 10 Polarization curves obtained in Ringer solution for different samples: (a) Ti−6Al−4V$_{0.50Mo}$; (b) Ti−6Al−4V$_{0.50P}$; (c) Ti−6Al−4V$_{0.025V}$; (d) Bare Ti−6Al−4V alloy (Sweep rate: 0.001 V/s; Potential range: −1.0 to 3.0 V (vs SCE); Insert: magnified zone of polarization curves in the potential range from 0.2 to 0.6 V)

density of the anodized samples is lower than that of the untreated alloy in this region. For a more precise study, chronoamperometry measurements were done at an applied potential of 0.5 V (vs Ag/AgCl) during 1 h in Ringer solution (Fig. 11). The results show a comparison of the corrosion behavior of the samples. It can be observed that the bare alloy registers the highest current density, ending the experience with a value of 15.34 μA/cm^2. Moreover, the anodized electrodes present current densities below 4 μA/cm^2, being Ti−6Al−4V$_{0.50Mo}$ the sample with the lowest value (1.34 μA/cm^2) revealing a better corrosion resistance than the untreated Ti−6Al−4V alloy in the range of the body potential.

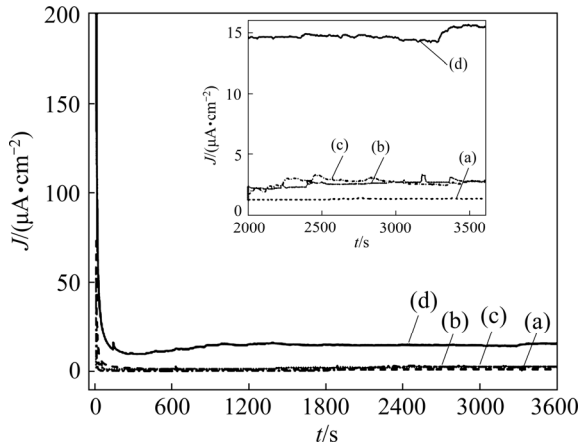

Fig. 11 Current density vs time transient curves obtained in Ringer solution at 0.5 V (vs Ag/AgCl) during 1 h for different samples: (a) Ti−6Al−4V$_{0.50Mo}$; (b) Ti−6Al−4V$_{0.50P}$; (c) Ti−6Al−4V$_{0.025V}$; (d) Bare Ti−6Al−4V (Insert: magnified zone of chronoamperometric curves in the period between 2000 and 3600 s)

For a deeper study of the corrosion performance of the electrodes, OCP was monitored during 168 h (Fig. 12). Changes in OCP values as a function of time in an aggressive medium can be used to estimate the protection degree of the coated substrates. The anodized oxide formed onto Ti−6Al−4V$_{0.50Mo}$ provides protection to the substrate during the complete experience, finishing with a voltage of −0.056 V (vs SCE). On the other hand, Ti−6Al−4V$_{0.50P}$ and Ti−6Al−4V$_{0.025V}$ produce an anodic shift in the early stage, which is related to an anodic protection mechanism, but the OCP sharply falls to values close to those of the bare electrode after the first immersion day. Particularly, Ti−6Al−4V$_{0.50P}$ undergoes the potential of the naked electrode after almost four days. Finally, Ti−6Al−4V$_{0.50P}$ and Ti−6Al−4V$_{0.025V}$ register a potential of −0.414 and −0.404 V (vs SCE), respectively after 168 h of immersion.

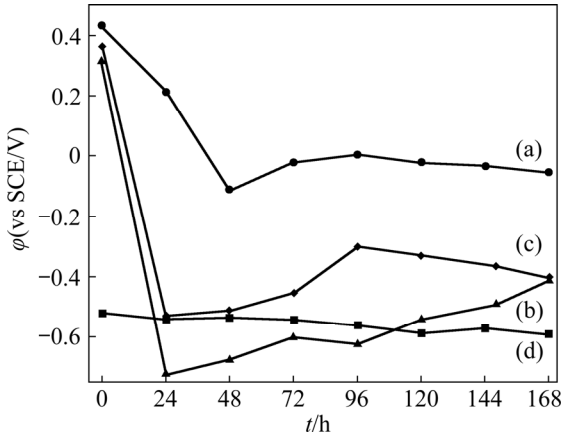

Fig. 12 Time dependence of OCP obtained in Ringer solution for different samples: (a) Ti−6Al−4V$_{0.50Mo}$; (b) Ti−6Al−4V$_{0.50P}$; (c) Ti−6Al−4V$_{0.025V}$; (d) Bare Ti−6Al−4V

In order to quantify analytically the corrosion protection of the coatings, the concentration of metal ions released during the last experience was determined using ICP-AES (Table 4). None of the samples released a significant concentration of ions. But it can be inferred that the inhibitor ions (Mo, P and V) were incorporated into the oxide layer during the anodization process due to the fact that the three inhibitor ions were detected in Ringer solution by this technique.

Table 4 Ions released after 168 h at OCP in Ringer solution

Sample	Ti	Al	V	Mo	P
Bare Ti−6Al−4V	<0.007	<0.005	0.006	−	−
Ti−6Al−4V$_{0.50Mo}$	<0.007	<0.005	0.002	0.214	−
Ti−6Al−4V$_{0.50P}$	<0.007	<0.005	0.004	−	0.067
Ti−6Al−4V$_{0.025V}$	<0.007	<0.005	0.028	−	−

The coatings were characterized by SEM and EDX after the prolonged immersion in Ringer solution. The SEM images of each electrode are shown in Fig. 13. The absence of cracks can be observed in the different oxides. Moreover, new deposits (indicated with arrows) are present on the surface of the treated samples after immersion (Figs. 13(b, c and d)).

In order to establish the nature of these deposits, EDX analyses were performed. Different elements were detected by EDX (Fig. 14). Na, K and Ca are identified on Ti−6Al−4$V_{0.50P}$, and Na, Cl and Ca in the case of Ti−6Al−4$V_{0.025V}$. The incorporation of the mentioned ions is possible due to the presence of the OH-bridges formed on the surface of titanium during hydroxylation. These bridges are highly polarized and an exchange with the cations available in the environment is

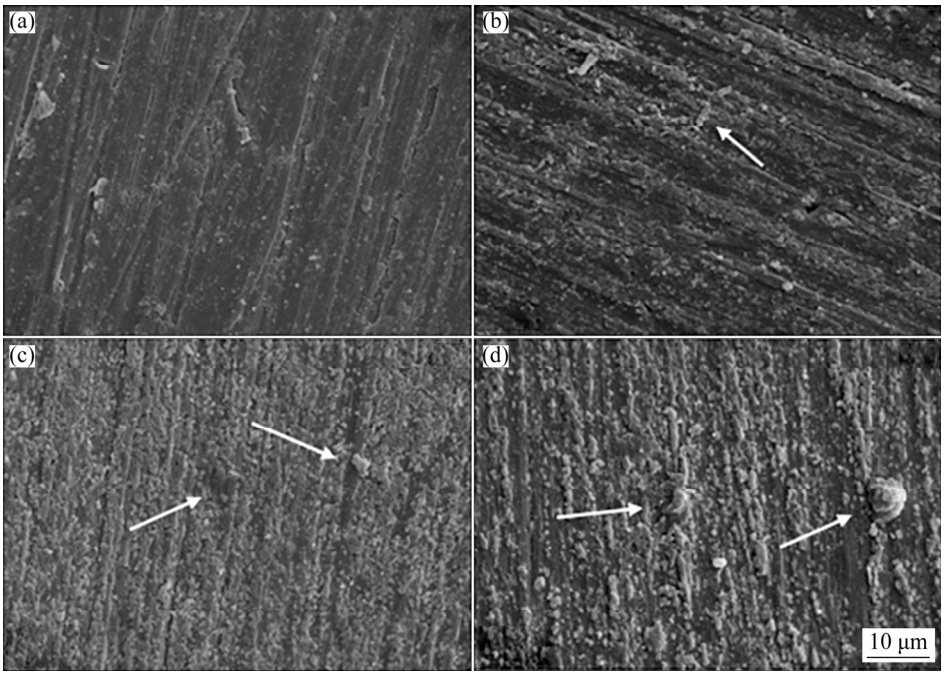

Fig. 13 SEM images for mechanically abraded Ti−6Al−4V (a), Ti−6Al−4$V_{0.50Mo}$ (b), Ti−6Al−4$V_{0.50P}$ (c) and Ti−6Al−4$V_{0.025V}$ (d) after 168 h in Ringer solution

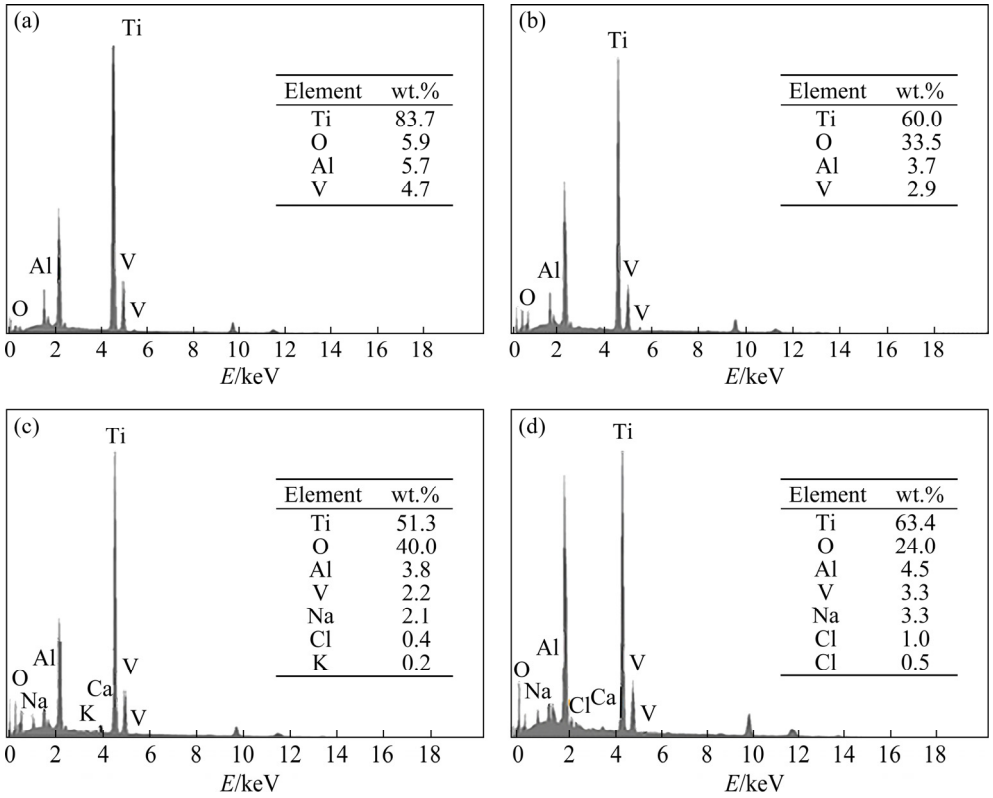

Fig. 14 EDX spectra for mechanically abraded Ti−6Al−4V (a), Ti−6Al−4$V_{0.50Mo}$ (b), Ti−6Al−4$V_{0.50P}$ (c), and Ti−6Al−4$V_{0.025V}$ (d) after 168 h in Ringer solution

promoted [51,52]. Chloride ions present in the Ringer solution can be adsorbed on the alloy surface, resulting in the formation of the chemisorbed complex $[TiCl_4]^{4-}$ [51,53]. The presence of the chlorine complex evidences the dissolution of the TiO_2 film. On the other hand, Ti−6Al−4$V_{0.50Mo}$ only exhibits the Ti, Al, V and O signals. The absence of chlorine indicates a good corrosion resistance. In conclusion, it is suggested that the deposits observed in the SEM image of Ti−6Al−4$V_{0.50Mo}$ are constituted by TiO_2 while for Ti−6Al−4$V_{0.50P}$ and Ti−6Al−4$V_{0.025V}$, the deposits also contain ions from Ringer solution.

The superior results for Ti−6Al−4$V_{0.50Mo}$ are due to the fact that Mo is a known corrosion inhibitor for several metals and alloys [54,55]. The anion reduces the passivity current and extends the passive range. The different molybdenum species incorporated into the oxide film act as corrosion inhibitors, which prevents the dissolution of Ti−6Al−4V alloy by forming a barrier film. The anions inhibit chloride ions adsorption present in Ringer solution and the molybdenum anion-rich regions on the coating retard chloride ions ingress to the alloy/oxide interface.

4 Conclusions

(1) The alloy surface was completely covered by the formed oxides and no cracks were detected. Ti−6Al−4$V_{0.50Mo}$ showed a more compact morphology compared to Ti−6Al−4$V_{0.50P}$ and Ti−6Al−4$V_{0.025V}$.

(2) Ti and O were the main constituent elements of the three anodized oxides, and XRD patterns confirmed the amorphous character of the titanium oxides.

(3) The incorporation of Mo, V and P was detected by the release of each ion through ICP-AES analysis.

(4) The presence of inhibitor ions in the anodization solutions produced a shift in the φ_{corr} to more positive values and for Ti−6Al−4$V_{0.50Mo}$ and Ti−6Al−4$V_{0.50P}$, a decrease in the J_{corr} values was also obtained.

(5) Chronoamperometries performed at the body potential demonstrate that the lowest current density was achieved for Ti−6Al−4$V_{0.50Mo}$. This oxide was able to protect the alloy in Ringer solution during 168 h and no corrosion products were detected on the surface after the immersion.

(6) Ti−6Al−4$V_{0.50Mo}$ electrode showed the best anticorrosive properties in simulated physiological solution, the incorporation of Mo^{4+} and Mo^{6+} in the oxide film inhibited chloride ions adsorption present in Ringer solution preventing the dissolution of the alloy.

Acknowledgments

The financial supports of the Secretaría de Ciencia y Técnica-UNS (PGI 24/M159), the Consejo Nacional de Investigaciones Científicas y Técnicas (CONICET-PIP 112-20150-100147) and the Agencia Nacional de Promoción Científica y Tecnológica (ANPCyT-PICT 2015-0726) are gratefully acknowledged.

References

[1] SAMARAS T. Longevity of specific populations [M]. 2nd ed. Amsterdam: Elsevier, 2017.

[2] MOHAMMED M T, KHAN Z A, SIDDIQUEE A N. Beta titanium alloys: The lowest elastic modulus for biomedical applications: A review [J]. International Journal of Chemical, Nuclear, Metallurgical and Materials Engineering, 2014, 8: 726−731.

[3] SITTIG C, TEXTOR M, SPENCER N D, WIELAND M, VALLOTTON P H. Surface characterization of implant materials c.p. Ti, Ti−6Al−7Nb and Ti−6Al−4V with different pretreatments [J]. Journal of Materials Science: Materials in Medicine, 1999, 10: 35−46.

[4] LIU S Y, SHIN Y C. Additive manufacturing of Ti6Al4V alloy: A review [J]. Materials & Design, 2019, 164: 107552.

[5] GURRAPPA I. Characterization of titanium alloy Ti−6Al−4V for chemical, marine and industrial applications [J]. Materials Characterization, 2003, 51: 131−139.

[6] CHEN H C, PINKERTON A J, LI L. Fibre laser welding of dissimilar alloys of Ti−6Al−4V and Inconel 718 for aerospace applications [J]. The International Journal of Advanced Manufacturing Technology, 2011, 52: 977−987.

[7] AHMED Y, SALLEH K, SAHARI M, ISHAK M, KHIDHIR B. Titanium and its alloy [J]. International Journal of Science and Research, 2014, 3: 1351−1361.

[8] KOIZUMI H, TAKEUCHI Y, IMAI H, KAWAI T, YONEYAMA T. Application of titanium and titanium alloys to fixed dental prostheses [J]. Journal of Prosthodontic Research, 2019, 63: 266−270.

[9] RENGANATHAN G, TANNERU N, MADURAI S L. Orthopedical and biomedical applications of titanium and zirconium metals [M]//Fundamental Biomaterials: Metals. Amsterdam: Elsevier, 2018: 211−241.

[10] CHOUBEY A, BALASUBRAMANIAM R, BASU B. Effect of replacement of V by Nb and Fe on the electrochemical and corrosion behavior of Ti−6Al−4V in simulated physiological environment [J]. Journal of Alloys and

Compounds, 2004, 381: 288−294.

[11] KHADIJA G, SALEEM A, AKHTAR Z, NAQVI Z, GULL M, MASOOD M, MUKHTAR S, BATOOL M, SALEEM N, RASHEED T, NIZAM N, IBRAHIM A, IQBAL F. Short term exposure to titanium, aluminum and vanadium (Ti6Al4V) alloy powder drastically affects behavior and antioxidant metabolites in vital organs of male albino mice [J]. Toxicology Reports, 2018, 5: 765−770.

[12] WALKER P R, LEBLANC J, SIKORSKA M. Effects of aluminum and other cations on the structure of brain and liver chromatin [J]. Biochemistry, 1989, 28: 3911−3915.

[13] LI J, LIU X. Chemical surface modification of metallic biomaterials [M]//Surface Coating and Modification of Metallic Biomaterials. Amsterdan: Elsevier, 2015: 159−183.

[14] JU Jiang, LI Jing-jing, JIANG Min, LI Meng-ya, YANG Li-xiang, WANG Kai-ming, YANG Chao, KANG Mao-dong, WANG Jun. Microstructure and electrochemical corrosion behavior of selective laser melted Ti−6Al−4V alloy in simulated artificial saliva [J]. Transactions of Nonferrous Metals Society of China, 2021, 31: 167−177.

[15] MOKGALAKA M N, POPOOLA A P I, PITYANA S L. In situ laser deposition of NiTi intermetallics for corrosion improvement of Ti−6Al−4V alloy [J]. Transactions of Nonferrous Metals Society of China, 2015, 25: 3315−3322.

[16] SUBRAMANI K, AHMED W. Titanium nanotubes as carriers of osteogenic growth factors and antibacterial drugs for applications in dental implantology [M]//Emerging Nanotechnologies in Dentistry. Amsterdam: Elsevier, 2012: 103−111.

[17] YAO C, LU J, WEBSTER T. Titanium and cobalt−chromium alloys for hips and knees [M]. Sawston: Woodhead Publishing, 2010.

[18] PRANDO D, BRENNA A, DIAMANTI M V, BERETTA S, BOLZONI F, ORMELLESE M, PEDEFERRI M. Corrosion of titanium: Part 2: Effects of surface treatments [J]. Journal of Applied Biomaterials & Functional Materials, 2018, 16: 3−13.

[19] PEDEFERRI M. Titanium anodic oxidation: A powerful technique for tailoring surfaces properties for biomedical applications [C]//144th Annual Meeting & Exhibition. Cham: TMS, 2015: 515−520.

[20] DIAMANTI M V, DEL CURTO B, PEDEFERRI M. Anodic oxidation of titanium: From technical aspects to biomedical applications [J]. Journal of Applied Biomaterials & Biomechanics: JABB, 2011, 9: 55−69.

[21] MOGODA A S, AHMAD Y H, BADAWY W A. Corrosion inhibition of Ti−6Al−4V alloy in sulfuric and hydrochloric acid solutions using inorganic passivators [J]. Materials and Corrosion, 2004, 55: 449−456.

[22] NARAYANAN R, SESHADRI S K. Phosphoric acid anodization of Ti−6Al−4V—Structural and corrosion aspects [J]. Corrosion Science, 2007, 49: 542−558.

[23] KRASICKA-CYDZIK E. Tailoring of anodic surface layer properties on titanium and its implant alloys for biomedical purposes [J]. Journal of Achievements in Materials and Manufacturing Engineering, 2010, 43: 424−431.

[24] PAUL S, YADAV K. Corrosion behavior of surface-treated implant Ti−6Al−4V by electrochemical polarization and impedance studies [J]. Journal of Materials Engineering and Performance, 2011, 20: 422−435.

[25] PÁEZ M A, FOONG T M, NI C T, THOMPSON G E, SHIMIZU K, HABAZAKI H, SKELDON P, WOOD G C. Barrier-type anodic film formation on an Al−3.5wt.%Cu alloy [J]. Corrosion Science, 1996, 38: 59−72.

[26] REHIM S A A, HASSAN H, AMIN M. Galvanostatic anodization of pure Al in some aqueous acid solutions. Part I: Growth kinetics, composition and morphological structure of porous and barrier-type anodic alumina films [J]. Journal of Applied Electrochemistry, 2002, 32: 1257−1264.

[27] van OVERMEERE Q, PROOST J. Stress-induced breakdown during galvanostatic anodising of zirconium [J]. Electrochimica Acta, 2010, 55: 4653−4660.

[28] KARAMBAKHSH A, AFSHAR A, GHAHRAMANI S, MALEKINEJAD P. Pure commercial titanium color anodizing and corrosion resistance [J]. Journal of Materials Engineering and Performance, 2011, 20: 1690−1696.

[29] SUL Y T, JOHANSSON C B, JEONG Y, ALBREKTSSON T. The electrochemical oxide growth behaviour on titanium in acid and alkaline electrolytes [J]. Medical Engineering & Physics, 2001, 23: 329−346.

[30] DIAMANTI M V, SPREAFICO F C, PEDEFERRI M P. Production of anodic TiO_2 nanofilms and their characterization [J]. Physics Procedia, 2013, 40: 30−37.

[31] GUILLÉN E, KRAUSE M, HERAS I, RINCÓN-LLORENTE G, ESCOBAR-GALINDO R. Tailoring crystalline structure of titanium oxide films for optical applications using non-biased filtered cathodic vacuum arc deposition at room temperature [J]. Coatings, 2021, 11: 233.

[32] DIAMANTI M V, ORMELLESE M, PEDEFERRI M. Application-wise nanostructuring of anodic films on titanium: A review [J]. Journal of Experimental Nanoscience, 2015, 10: 1285−1308.

[33] ZHOU W L, APKARIAN R, WANG Z L, JOY D. Fundamentals of scanning electron microscopy (SEM) [M]. New York: Springer, 2007.

[34] MARTÍNEZ C, GUERRA C, SILVA D, CUBILLOS M, BRIONES F, MUÑOZ L, PÁEZ M A, AGUILAR C, SANCY M. Effect of porosity on mechanical and electrochemical properties of Ti−6Al−4V alloy [J]. Electrochimica Acta, 2020, 338: 135858.

[35] MILOŠEV I, METIKOŠ-HUKOVIĆ M, STREHBLOW H. Passive film on orthopaedic TiAlV alloy formed in physiological solution investigated by X-ray photoelectron spectroscopy [J]. Biomaterials, 2000, 21: 2103−2113.

[36] VINCENT CRIST B. Handbook of monochromatic XPS spectra [M]. California: XPS International L.L.C., 2005.

[37] SUNDARARAJAN T, KAMACHI MUDALI U, NAIR K G M, RAJESWARI S, SUBBAIYAN M. Surface characterization of electrochemically formed passive film on nitrogen ion implanted Ti6Al4V alloy [J]. Materials Transactions, JIM, 1998, 39: 756−761.

[38] HIERRO-OLIVA M, GALLARDO-MORENO A M, GONZÁLEZ-MARTÍN M L. XPS analysis of Ti6Al4V oxidation under UHV conditions [J]. Metallurgical and Materials Transactions A, 2014, 45: 6285−6290.

[39] BIESINGER M C, LAU L W M, GERSON A R, SMART R S C. Resolving surface chemical states in XPS analysis of first row transition metals, oxides and hydroxides: Cr, Mn,

Fe, Co and Ni [J]. Applied Surface Science, 2011, 257: 2717−2730.
[40] SILVA D, GUERRA C, MUÑOZ H, AGUILAR C, WALTER M, AZOCAR M, MUÑOZ L, GÜRBÜZ E, RINGUEDÉ A, CASSIR M, SANCY M. The effect of Staphylococcus aureus on the electrochemical behavior of porous Ti−6Al−4V alloy [J]. Bioelectrochemistry, 2020, 136: 107622.
[41] KAR A, RAJA K S, MISRA M. Electrodeposition of hydroxyapatite onto nanotubular TiO_2 for implant applications [J]. Surface and Coatings Technology, 2006, 201: 3723−3731.
[42] GHICOV A, TSUCHIYA H, MACAK J M, SCHMUKI P. Titanium oxide nanotubes prepared in phosphate electrolytes [J]. Electrochemistry Communications, 2005, 7: 505−509.
[43] MU S L, DU J, JIANG H, LI W F. Composition analysis and corrosion performance of a Mo−Ce conversion coating on AZ91 magnesium alloy [J]. Surface and Coatings Technology, 2014, 254: 364−370.
[44] CAI Z, SHAFER T, WATANABE I, NUNN M E, OKABE T. Electrochemical characterization of cast titanium alloys [J]. Biomaterials, 2003, 24: 213−218.
[45] LÓPEZ M F, GUTIÉRREZ A, JIMÉNEZ J A. In vitro corrosion behaviour of titanium alloys without vanadium [J]. Electrochimica Acta, 2002, 47: 1359−1364.
[46] ROBIN A, CARVALHO O A S, SCHNEIDER S G, SCHNEIDER S. Corrosion behavior of Ti−*x*Nb−13Zr alloys in Ringer's solution [J]. Materials and Corrosion, 2008, 59: 929−933.
[47] MCCAFFERTY E. Validation of corrosion rates measured by the Tafel extrapolation method [J]. Corrosion Science, 2005, 47: 3202−3215.
[48] BOBIC B, BAJAT J, ACIMOVIC-PAVLOVIC Z, RAKIN M, BOBIC I. The effect of T4 heat treatment on the microstructure and corrosion behaviour of Zn27Al1.5-Cu0.02Mg alloy [J]. Corrosion Science, 2011, 53: 409−417.
[49] BERBEL L O, BANCZEK E D P, KAROUSSIS I K, KOTSAKIS G A, COSTA I. Determinants of corrosion resistance of Ti−6Al−4V alloy dental implants in an in Vitro model of peri-implant inflammation [J]. PLoS One, 2019, 14: e0210530.
[50] VELTEN D, BIEHL V, AUBERTIN F, VALESKE B, POSSART W, BREME J. Preparation of TiO_2 layers on cp-Ti and Ti6Al4V by thermal and anodic oxidation and by sol−gel coating techniques and their characterization [J]. Journal of Biomedical Materials Research, 2002, 59: 18−28.
[51] RADOVANOVIĆ M B, TASIĆ Ž Z, SIMONOVIĆ A T, PETROVIĆ MIHAJLOVIĆ M B, ANTONIJEVIĆ M M. Corrosion behavior of titanium in simulated body solutions with the addition of biomolecules [J]. ACS Omega, 2020, 5: 12768−12776.
[52] BROWNE M B, GREGSON P J. Surface modification of titanium alloy implants [J]. Biomaterials, 1994, 15: 894−898.
[53] GONZÁLEZ J E G, MIRZA-ROSCA J C. Study of the corrosion behavior of titanium and some of its alloys for biomedical and dental implant applications [J]. Journal of Electroanalytical Chemistry, 1999, 471: 109−115.
[54] SHAMS EL DIN A M, MOHAMMED R A, HAGGAG H H. Corrosion inhibition by molybdate/polymaliate mixtures [J]. Desalination, 1997, 114: 85−95.
[55] SILVA J W J, CODARO E N, NAKAZATO R Z, HEIN L R O. Influence of chromate, molybdate and tungstate on pit formation in chloride medium [J]. Applied Surface Science, 2005, 252: 1117−1122.

缓蚀离子存在条件下阳极氧化提高 Ti−6Al−4V 合金的耐蚀性

A. L. MARTINEZ[1,2], D. O. FLAMINI[1,2], S. B. SAIDMAN[1,2]

1. Instituto de Ingeniería Electroquímica y Corrosión (INIEC), Departamento de Ingeniería Química (DIQ), Universidad Nacional del Sur (UNS), Argentina;
2. Consejo Nacional de Investigaciones Científicas y Técnicas (CONICET), Bahía Blanca, Argentina

摘　要：通过恒电流阳极氧化在 Ti−6Al−4V 合金表面制备彩色氧化物薄膜。采用 3 种不同的含有腐蚀无机缓蚀剂的水溶液(Na_2MoO_4，NaH_2PO_4 和 NH_4VO_3)进行阳极化处理，研究缓蚀剂阴离子对合金在 Ringer 溶液中腐蚀行为的影响。采用开路电位(OCP)、Tafel 极化、线性扫描伏安(LSV)和计时电流(CA)等手段，评估处理后电极的腐蚀性能。通过释放的 Mo、V 和 P，采用 ICP-AES 技术检测缓蚀剂离子的掺入。利用扫描电子显微镜(SEM)、X 射线衍射(XRD)和 X 射线光电子能谱(XPS)对形成的氧化物进行表征。结果表明，无论采用何种溶液，均获得无孔或裂纹的致密无定形氧化物。在 Na_2MoO_4 溶液中阳极氧化样品的腐蚀电流密度最低(0.11 μA/cm^2)，即使在 Ringer 溶液中浸泡 168 h，仍能保护合金，而未检测到裂纹或腐蚀产物。XPS 分析结果显示，钼以 Mo^{6+}和 Mo^{4+}的形式掺入氧化膜中。

关键词：Ti−6Al−4V 合金；阳极氧化；无机缓蚀剂；腐蚀防护

(Edited by Xiang-qun LI)